Supporting information for

A pH-gradient Flow Cell for Converting Waste CO_2 into Electricity

Taeyoung Kim, Bruce E. Logan, and Christopher A. Gorski*

Department of Civil and Environmental Engineering, The Pennsylvania State University, University Park, PA 16802, USA
*Corresponding Author: gorski@engr.psu.edu;
+1-814-865-5673 (phone), +1-814-863-7304 (Fax)

A. Characterization of manganese oxide powder

Scanning electron microscope (SEM) images of MnO_2 powders were collected using a Nova NanoSEM 630 (FEI Corporation, Hilsboro, OR). The samples was prepared by placing a small amount of powder on double-sided carbon tape that was adhered to an aluminum SEM stub. The sample was not sputter-coated. Transmission electron microscope (TEM) images were recorded using a Talos microscope (FEI Corporation, Hilsboro, OR) at 200 keV. The MnO_2 powder was first mixed with ethanol, then two drops of the resulting mixture were loaded on a lacy carbon grid (Electron Microscopy Sciences, 200 mesh Cu grid). The MnO_2 prepared by co-precipitation method formed a large cluster consisting of small particles (Figure S1). The diameters of individual particles within larger aggregates were approximately 100 to 200 nm based on visual inspection of the images. We were unable to quantify the particle size distributions because significant overlap among individual particles in the images made measuring the majority of particles technically infeasible.

An X-ray diffraction (XRD) pattern of the MnO_2 powder was obtained by using a PANalytical Empryean X-Ray Diffractometer in the scan range between 5 and 70 degrees 2θ with a Cu kα source. The XRD pattern confirms that the synthesized MnO_2 particles using a co-precipitation method were amorphous or very poorly crystalline form (Figure S2), in good agreement with a previously reported XRD pattern for an MnO_2 sample prepared using the same co-precipitation method.[1, 2]

Nitrogen adsorption/desorption isotherms were recorded using a Micromeritics ASAP 2420 (Figure S3). BET surface area of the sample was 158.5±0.4 m^2/g, and pore volume was 0.189 cm^3/g (BJH desorption cumulative volume).

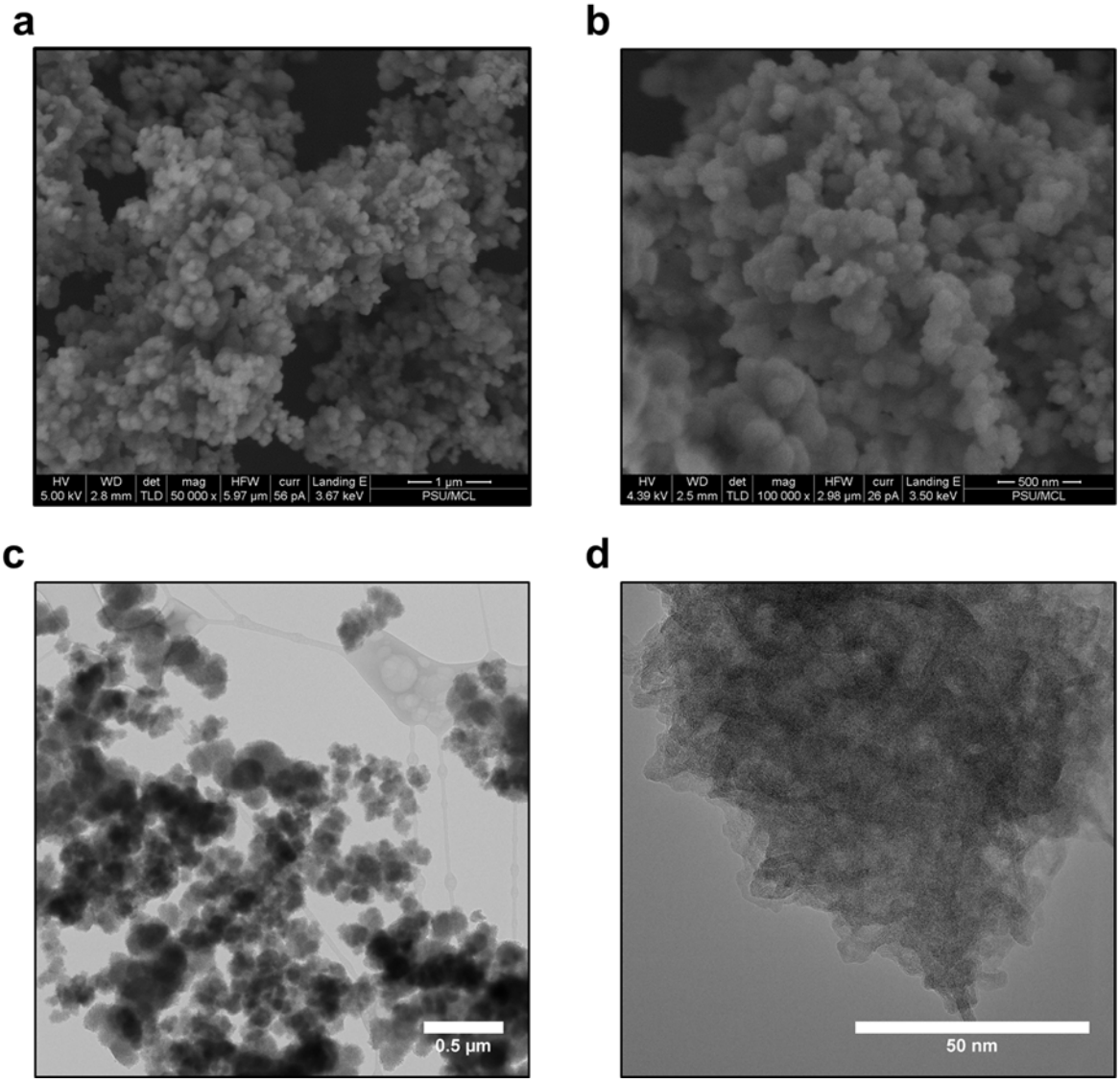

Figure S1. (a, b) Scanning electron microscope (SEM) and (c, d) transmission electron microscope (TEM) images of MnO_2 particles.

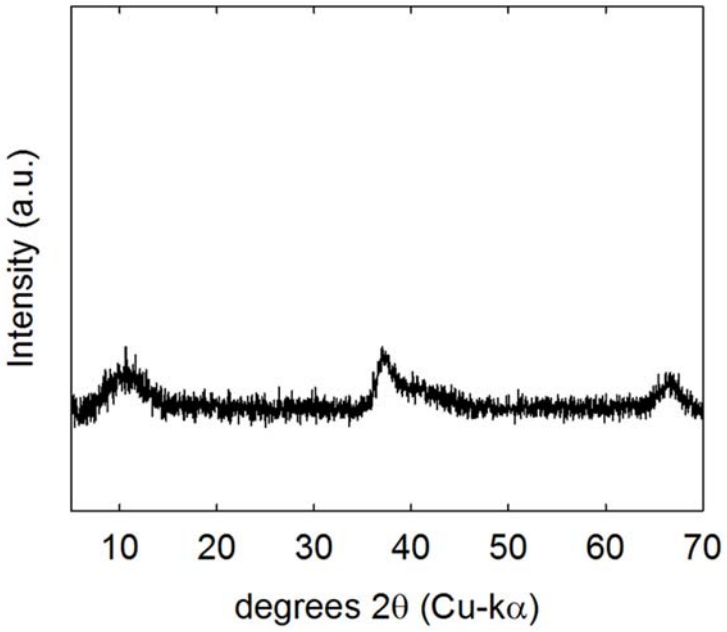

Figure S2. X-ray diffraction (XRD) pattern of MnO_2.

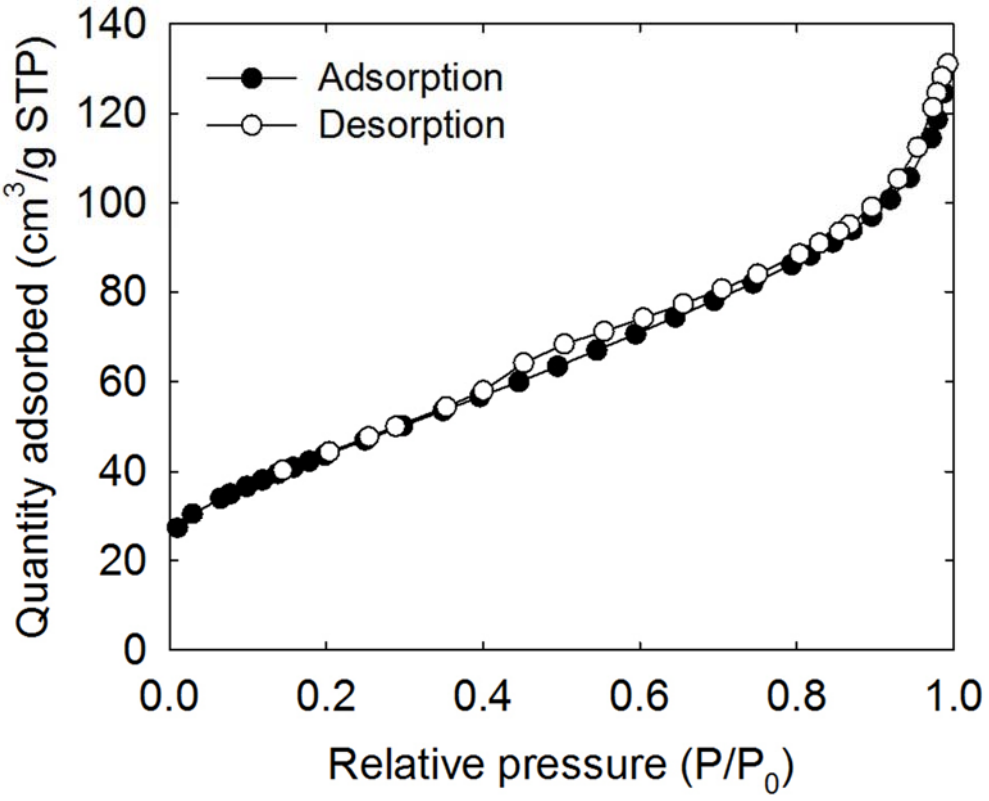

Figure S3. Nitrogen adsorption/desorption isotherms of MnO_2. BET surface area of the sample was 158.5±0.4 m^2/g.

B. Flow cell construction

A custom-built flow cell consisted of two channels that were simultaneously fed by two aqueous solutions sparged with either a high CO_2 partial pressure (to represent exhaust gas) or a low CO_2 partial pressure (to represent ambient air). Each solution was injected into a hole located at the bottom of the cell, which flowed vertically upwards to the top of the cell through two rectangular channels (area = ~3 cm^2, thickness = 200 μm, volume = 0.06 mL). A non-selective membrane (Celgard® 3501, pore size = 0.064 μm, thickness = 25 μm) was placed between the two channels, which prevented instantaneous mixing between the two solutions. We selected this membrane as it produces a low resistance due to surfactant-aided hydrophilicity (based on specification provided by company) and its small pore size could separate the pH difference between two flow channels. The MnO_2 electrodes were placed in each channel, and a graphite foil behind each electrode served as a current collector. The cell was sealed using two end plates with bolts and nuts.

C. Measuring electrode potential as a function of pH

The electrode potential of MnO_2 electrode was measured in a 3-electrode cell with a platinum wire counter electrode and an Ag/AgCl (3 M NaCl) reference electrode. The electrode potential was first set to 0.3 V vs. Ag/AgCl by applying constant potential until the current decreased to approximately 0.1 mA in a 1 M $NaHCO_3$ solution (pH = 8.1). Afterwards, the open-circuit potential was measured as a function of pH, ranging from 7.7 (1 M $NaHCO_3$ sparged with CO_2) to 11.9 (0.5 M Na_2CO_3). Intermediate pH values were achieved by mixing the two solutions in different ratios. We selected these solution concentrations to maintain a constant 1 M Na^+ concentration.

D. Estimating the highest power density achievable in the system

To estimate the highest power density achievable in this system, we performed additional experiments in which we prepared solutions with larger pH differences. We calculated that the highest achievable pH difference for 1 M $NaHCO_3$ solutions in equilibrium either with pure CO_2 (pCO_2 = 1 atm) or ambient air (pCO_2 = 0.00038 atm) was approximately 2.4, if the solutions reached equilibrium with the gas phase (Fig. S4a). This value was larger than the pH difference we achieved in our sparging experiments (i.e., 1.7) because we stopped sparging the solutions before they reached equilibrium. When we prepared solutions with this larger pH difference, the cell voltage increased from 0.199 V to 0.281 V (Fig. S4b) and the power density increased from 0.82 W/m^2 to 1.70 W/m^2 at R_{ext} = 6 Ω (Fig. S4c and d).

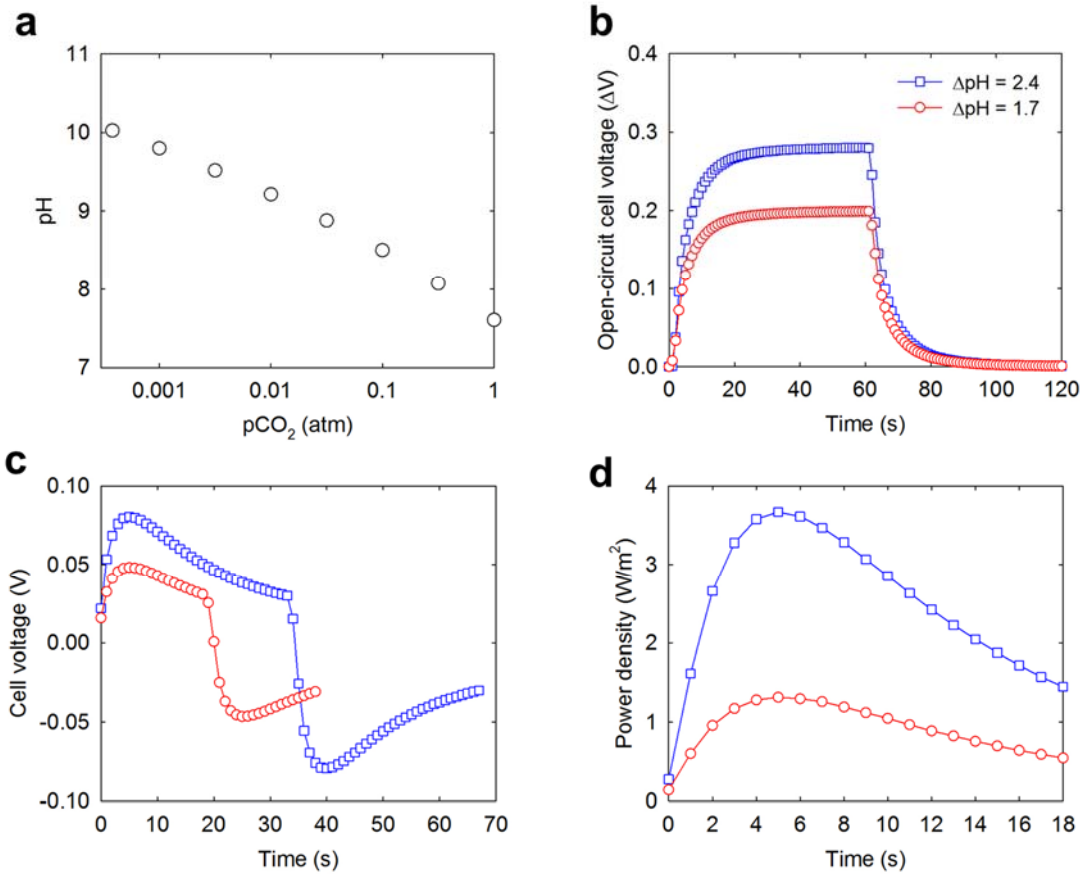

Figure S4. (a) Equilibrium pH values of 1 M $NaHCO_3$ depending on CO_2 partial pressure. The calculation was conducted by using Visual MINTEQ software (Davies equation), and the resulting pH values were 10.03 at 0.00038 atm (atmospheric condition) and 7.61 at 1 atm. (b) Open-circuit cell voltage, (c) cell voltage, and (d) power density profiles recorded using 1 M $NaHCO_3$ solutions with the pH difference of 1.7 (this study) and 2.4 (maximum ΔpH). The open-circuit cell voltage differences were approximately 0.199 (ΔpH = 1.7) and 0.281 V (ΔpH = 2.4). Power production was achieved at R_{ext} = 6 Ω, which produced 0.82 (ΔpH = 1.7) and 1.70 W/m^2 (ΔpH = 2.4) from two representative cycles.

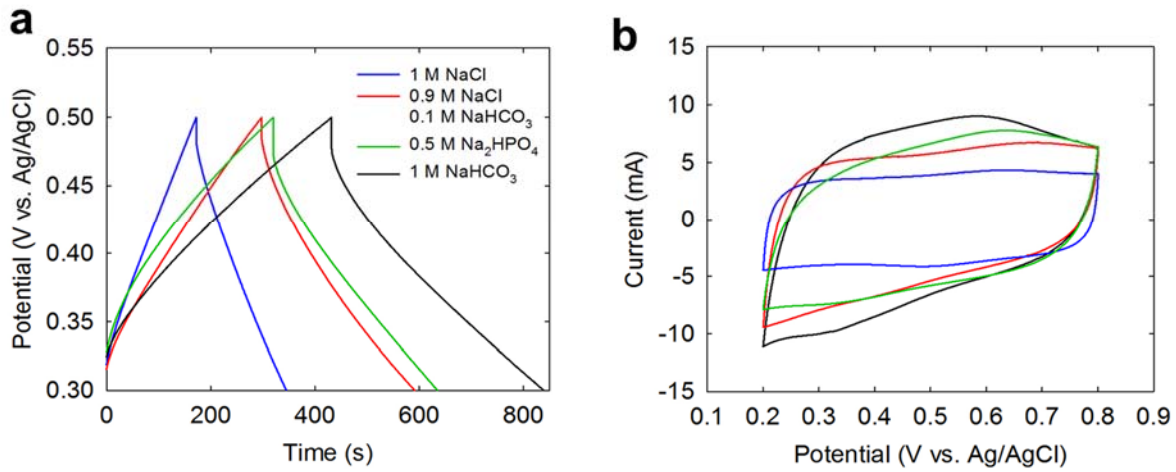

Figure S5. (a) Galvanostatic charge/discharge and (b) cyclic voltammetry profiles of MnO_2 electrode in several sodium-based solutions. For the galvanostatic charge/discharge tests, potential profiles were recorded while applying constant current of ±0.5 mA/cm^2 between 0.3 and 0.5 V (vs. Ag/AgCl). The solution pH was adjusted to approximately 8.3 by adding 0.1 M NaOH (1 M NaCl), 0.1 M HCl (0.5 M Na_2HPO_4), or sparging air (1 M $NaHCO_3$). The conductivity values of each solution were 51.5 mS/cm (1 M $NaHCO_3$), 81.0 mS/cm (0.1 M $NaHCO_3$ and 0.9 M NaCl), 84.6 mS/cm (1 M NaCl), and 41.3 mS/cm (0.5 M Na_2HPO_4). The cycle voltammetry was conducted in the potential range between 0.2 and 0.8 V (vs. Ag/AgCl) at the scan rate of 1 mV/s. The solution pH was adjusted to approximately 8.

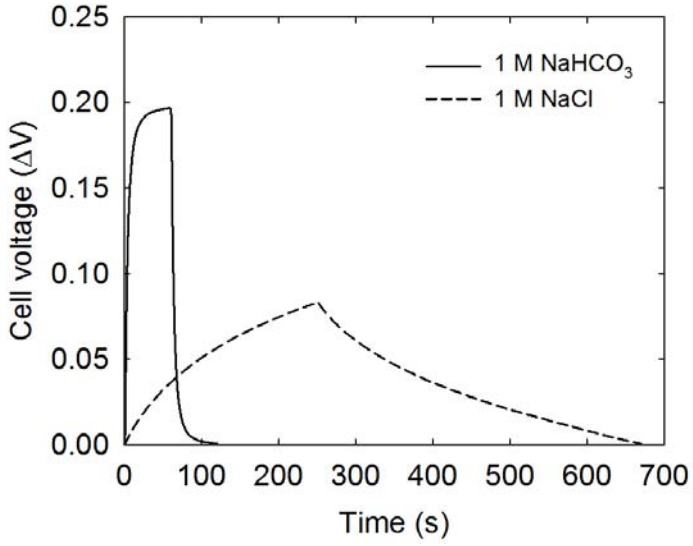

Figure S6. Open-circuit cell voltage profiles of 1 M $NaHCO_3$ (solid line) and 1 M NaCl in the pH-gradient flow cell with two MnO_2 electrodes. The pH difference between two solutions injected to the flow cell was 1.7, which was adjusted by sparging CO_2 and air (1 M $NaHCO_3$) or adding 0.1 M NaOH solution (1 M NaCl). The flow path of two solutions was switched at 60 s (1 M $NaHCO_3$) or 250 s (1 M NaCl). The flow rate was 15 ml/min.

E. Energy calculations

To evaluate the theoretical energy that can be achieved by mixing high and low pH 1 M $NaHCO_3$ solutions, we obtained the concentration and activity of each component before and after the mixing by using Visual MINTEQ software (Table S1). When mixed the same volume (1 L) of two 1 M $NaHCO_3$ solutions at pH 7.7 (pCO_2 = 0.8 atm) and 9.4 (pCO_2 = 0.005 atm), the resulting pH achieved was 8.74. Using concentration and/or activity of each component allowed us to calculate the Gibbs free energy of mixing according the following equation:[3, 4]

$$\Delta G_{mix} = RT \sum_i [c_{i,h} V_h \ln(\gamma_{i,h} c_{i,h}) + c_{i,l} V_l ln(\gamma_{i,l} c_{i,l}) - c_{i,m} V_m ln(\gamma_{i,m} c_{i,m})]$$

where ΔG_{mix} is the difference in the Gibbs free energy of mixing (J), c is the concentration (M), γ is the activity coefficient, R is the gas constant (8.314 J mol^{-1} K^{-1}), T is the temperature (298 K), V is the volume (L), subscript h is the high pH, subscript l is the low pH, and subscript m is the mixed solution. The resulting mixing energy per a liter of the mixed solution was 0.295 kJ/L when activity-corrected values (Davies equation) were used, and 0.287 kJ/L when we assumed that activity coefficients are unity. Normalizing this theoretical mixing energy (0.295 kJ/L) to the amount of CO_2 produced 76.8 kJ/kg CO_2 gas. This value was calculated from the $TotCO_3$ concentration difference between CO_2-sparged (pH 7.7) and mixed (pH 8.74) solutions provided in Table S1, which was 0.175 M, because CO_2 was needed to decrease the pH from the mixed solution to CO_2-sparged solution under our experimental condition. For 1 L of CO_2-sparged solution, 0.175 mol or 7.7 g of CO_2 was needed to change pH, while the theoretical mixing energy available by mixing each 1 L of CO_2- and air-sparged solutions was 0.591 kJ (0.295 kJ/L of mixed solution)..

To determine whether sparging CO_2 is a feasible method to achieve pH gradients, we performed an experiment to estimate energy required for sparging CO_2. We made assumptions

for calculating this energy: (1) sparging CO_2 is needed to decrease pH from 8.74 (mixed solution) to 7.7 (low pH solution); (2) energy is not needed to increase pH because the solution can be equilibrated to the atmospheric CO_2 partial pressure (0.00038 atm) that is much smaller than the CO_2 partial pressure (0.005 atm) required to achieve pH 9.4 for 1 M $NaHCO_3$. A diffusion stone with 2 μm pores was located at the bottom of a glass bottle containing 0.5 L of 1 M $NaHCO_3$ (pH 8.7). The solution pH was monitored while sparging CO_2 gas (approximately 4 psi and 0.5 L/min) under vigorous stirring at room temperature. The time it took to reach pH 7.7 was approximately 2 min. The pressure, flow rate, and time allowed us to calculate the energy consumed to adjust pH from 8.7 to 7.7, which was approximately 0.055 kJ/L. This energy is 19% of the theoretical energy of mixing calculated above (0.295 kJ/L). The contribution of the energy required for sparging CO_2 gas was in the similar range as the energy required in reverse-electrodialysis (RED) for pumping, which was 25% of the overall energy generated in a system producing power density of 0.8 W/m^2.[5]

Table S1. Concentration and activity values of each component for solutions before and after the mixing.

Component	Concentration (M)			Activity		
	pH 7.7	pH 9.4	pH 8.74	pH 7.7	pH 9.4	pH 8.74
	1 L	1 L	2 L	1 L	1 L	2 L
H_2CO_3 (aq)	0.023	0.000	0.001	0.027	0.000	0.002
HCO_3^-	0.791	0.253	0.543	0.605	0.191	0.412
$NaHCO_3$ (aq)	0.157	0.041	0.099	0.190	0.049	0.118
CO_3^{2-}	0.004	0.070	0.032	0.001	0.023	0.011
$NaCO_3^-$	0.022	0.283	0.148	0.017	0.214	0.112
H^+	2.62×10^{-8}	5.26×10^{-10}	2.42×10^{-9}	2.00×10^{-8}	3.97×10^{-10}	1.83×10^{-9}
OH^-	6.58×10^{-7}	3.36×10^{-5}	7.01×10^{-6}	5.03×10^{-7}	2.54×10^{-5}	5.32×10^{-6}
NaOH (aq)	3.29×10^{-7}	1.37×10^{-5}	3.20×10^{-6}	3.97×10^{-7}	1.63×10^{-5}	3.83×10^{-6}
Na^+	0.821	0.676	0.754	0.628	0.510	0.572

References

(1) Zhai, D.; Li, B.; Xu, C.; Du, H.; He, Y.; Wei, C.; Kang, F., A study on charge storage mechanism of α-MnO 2 by occupying tunnels with metal cations (Ba 2+, K+). *J. Power Sources* **2011,** *196*, (18), 7860-7867.

(2) Brousse, T.; Toupin, M.; Dugas, R.; Athouël, L.; Crosnier, O.; Bélanger, D., Crystalline MnO_2 as possible alternatives to amorphous compounds in electrochemical supercapacitors. *J. Electrochem. Soc.* **2006,** *153*, (12), A2171-A2180.

(3) Yip, N. Y.; Elimelech, M., Thermodynamic and energy efficiency analysis of power generation from natural salinity gradients by pressure retarded osmosis. *Environ. Sci. Technol.* **2012,** *46*, (9), 5230-5239.

(4) Post, J. W.; Veerman, J.; Hamelers, H. V.; Euverink, G. J.; Metz, S. J.; Nymeijer, K.; Buisman, C. J., Salinity-gradient power: Evaluation of pressure-retarded osmosis and reverse electrodialysis. *J. Membr. Sci.* **2007,** *288*, (1), 218-230.

(5) Veerman, J.; Saakes, M.; Metz, S.; Harmsen, G., Reverse electrodialysis: performance of a stack with 50 cells on the mixing of sea and river water. *J. Membr. Sci.* **2009,** *327*, (1), 136-144.